RAYS AND WAVES IN A PERIODICALLY PERTURBED PARALLEL PLATE WAVEGUIDE

by

R. P. Ratowsky and M. A. Lieberman

Memorandum No. UCB/ERL M88/59

29 August 1988

RAYS AND WAVES IN A PERIODICALLY PERTURBED PARALLEL PLATE WAVEGUIDE

by

R. P. Ratowsky and M. A. Lieberman

Memorandum No. UCB/ERL M88/59

29 August 1988

ELECTRONICS RESEARCH LABORATORY

College of Engineering
University of California, Berkeley
94720

RAYS AND WAVES IN A PERIODICALLY PERTURBED PARALLEL PLATE WAVEGUIDE

by

R. P. Ratowsky and M. A. Lieberman

Memorandum No. UCB/ERL M88/59

29 August 1988

ELECTRONICS RESEARCH LABORATORY

College of Engineering
University of California, Berkeley
94720

Rays and Waves in a Periodically Perturbed Parallel Plate Waveguide

R. P. Ratowsky
Department of Physics
University of California, Berkeley, CA 94720

M. A. Lieberman
Department of Electrical Engineering and Computer Sciences
University of California, Berkeley, CA 94720

ABSTRACT

Two related optical or acoustic systems are studied: a periodically perturbed two-dimensional waveguide and a periodic array of nonlinear lenses. The ray trajectories of the system are computed, using a Poincaré surface of section to study the dynamics. Each system leads to a near-integrable ray Hamiltonian: the phase space splits into regions showing regular or chaotic behavior. The solutions to the scalar Helmholtz equation are found via a secular equation determining the eigenfrequencies. A wave mapping is derived for the system in the paraxial regime. We find that localization of the waves occurs, limiting the beam spread in both wavevector and configuration space. We briefly consider the effect of higher order terms in the paraxial expansion on the wave mapping.

I. INTRODUCTION

This report addresses the issue of wave or quantum mechanical behavior for a simple system whose eikonal or classical limit displays the stochastic behavior generic to near-integrable Hamiltonian systems. Many model near-integrable systems have been considered in the literature, with the aim of studying the relation between quantum features (spectra, wavefunctions) and the classical phase space. Such studies have fallen into two general categories, distinguished by whether the underlying Hamiltonian is (1) constant in time or (2) periodic in time. Systems in both classes typically contain a parameter which carries the system from complete integrability to global stochasticity as this parameter is varied. For the integrable case, the theory relating classical orbits and wavefunctions is well known: stationary quantum states are based on invariant tori according to the prescription of Einstein-Brillouin-Keller (EBK) quantization [1]. When the tori are partially or completely destroyed, the situation is far less well understood: no complete theory exists. Thus numerical studies have become a crucial tool for understanding quantum states for systems whose classical limit is chaotic.

The model system we will study is one of physical importance: a parallel plate waveguide or duct with a periodically perturbed boundary (a grating). As we shall be interested in solutions to the scalar Helmholtz equation in the guide, various interpretations may be ascribed to the scalar wave in question. We may have in mind, for example, one component of an electromagnetic waveguide mode; the system then models a distributed feedback (DFB) laser or optical mode coupler [2,3]. Or the wavefunction may be interpreted as an acoustic velocity potential field; this system has certain device applications [4]. A third interpretation is that of an electron wavefunction in a periodic potential. Appropriate boundary conditions must be chosen for each case. All of these applications are interesting because they have been studied in the past without cognizance of the possibility of 'chaotic wavefunctions' which are suggested by the ray dynamics when strong stochasticity is present. Thus in certain regimes, perturbation schemes may yield misleading results, just as they would in the

classical case.

While the stationary states are of interest, our principal motivation for studying this system is to elucidate the relationship between autonomous and nonautonomous wave systems. Classically, it is frequently convenient to describe a bounded Hamiltonian system by a mapping, the Poincaré map, which samples the dynamics as orbits pierce a fixed surface of codimension two in the phase space. This mapping, generated by Hamilton's equations, is symplectic: phase volume is conserved [5]. An autonomous quantum or wave system may sometimes also be described by a mapping of the wave function, but only in an approximate sense. If the system wavevector spectrum is concentrated in a particular direction, and the properties of the medium vary only slowly in this direction, the paraxial approximation may be invoked and a unitary propagation operator may be found defining a quantum or wave mapping. The assumption of slow variation allows reflected waves to be ignored, which implies the unitarity of the propagator. We explicitly derive this unitary propagator for our waveguide system. The properties of the wave mapping have definite and surprising consequences for optical beam propagation in the system. In particular, the phenomenon of wavevector localization will be seen to apply to this system in certain important regimes.

Our study is divided into three parts. First we address the time independent problem of obtaining spectra and modal solutions in the waveguide system, to assess qualitatively the nature of the spectra and eigenmodes as a function of perturbation strength. Next we study the ray dynamics by means of an exact Poincaré surface of section mapping; we discuss an approximation to this mapping and obtain a criterion for global ray stochasticity. Finally, we derive the paraxial wave mapping, and deduce properties of the wave solution based on the dynamics generated by this mapping.

II. WAVEGUIDE SYSTEM

A. Geometry

The waveguide or cavity under consideration consists of two parallel planes separated by a distance H. Upon the lower plane rests a grating, of thickness h, whose density is chosen to be sinusoidal in the longitudinal coordinate x:

$$\rho(x) = \rho_0[1 + \eta \cos(K_w x)], \tag{1}$$

with wavenumber K_w. Here ρ_0 is the ambient density, and η is the modulation strength. The density for the region $h < z < H$ is ρ_1, which may differ from ρ_0. For solid media, ρ represents the ratio of mass density to the elastic stiffness constant; we may then think of the system as a uniform substrate region deposited with a film of periodic density. The origin of the transverse coordinate z is chosen so that the lower plane is coincident with $z = 0$ (See fig. 1). In general, we may think of equation (1) as the first two terms in the Fourier expansion of a density function.

Note that the above acoustical system may be equally well regarded as an electromagnetic one if the density is understood to be a dielectric function (with appropriate boundary conditions). Similarly, if $\rho(x)$ is considered to be a potential field, the problem has a quantum mechanical interpretation. In this report, we focus largely on the cases of scalar acoustics/optics and quantum mechanics.

B. Boundary Value Problem

For stationary states with time dependence $\exp(-i\omega t)$, the field $\psi(x, z)$ in each region satisfies the Helmholtz equation

$$\frac{\partial^2 \psi_\alpha}{\partial x^2}(x, z) + \frac{\partial^2 \psi_\alpha}{\partial z^2}(x, z) + k_\alpha^2(x)\psi_\alpha(x, z) = 0, \quad \alpha = 0, 1 \tag{2}$$

where

$$k_0^2(x) = k^2 \rho(x)$$

$$k_1^2(x) = k^2 \rho_1,$$

$k^2 = \omega^2/c_0^2$, and c_0 is the speed of sound. The subscripts 0 and 1 denote the fields in the grating and uniform region, respectively. For acoustic waves, the field $\psi(x,z)$ is related to the velocity field $\mathbf{v}(x,z)$ by $\rho(x)\mathbf{v}(x,z) = -\nabla\psi(x,z)$; equation (2) is exact for $\mathbf{v} \parallel \hat{\mathbf{y}}$, as is the case for horizontal shear acoustic waves. Otherwise, a term of order η has been neglected. For the electromagnetic case, equation (2) describes a TE waveguide mode with

$$\begin{aligned} \mathbf{E}(x,z) &= \psi(x,z)\hat{\mathbf{y}} \\ \mathbf{H}(x,z) &= -\frac{i}{\omega}\nabla \times \mathbf{E}, \end{aligned} \tag{3}$$

where $\hat{\mathbf{y}}$ is a unit vector in the transverse direction, c_0 the speed of light, and ρ is the dielectric function. Finally, for the quantum mechanical case we have

$$k_0^2 = \frac{2m}{\hbar^2}(E - V_\alpha(x)) = \begin{cases} k^2 - k_c^2\cos(K_w x), & \alpha = 0; \\ k^2, & \alpha = 1, \end{cases}$$

where $k^2 = 2mE/\hbar^2$ for a particle of energy E, and $k_c^2 = 2m\epsilon/\hbar^2$; $\epsilon = \eta\rho_0$ plays the role of the potential strength.

We will consider a class of problems defined by the boundary conditions taken at $z = 0$ and $z = H$. For a non-leaky (hard-wall) waveguide, the proper boundary conditions require the velocity field (wavefunction) to vanish at the walls and to be continuous across the interface. For a quantum system the wavefunction itself vanishes. Thus

$$\begin{aligned} \frac{\partial\psi_0}{\partial z}(x,0) &= \frac{\partial\psi_1}{\partial z}(x,H) = 0 \quad \text{(Acoustic)} \\ \psi_0(x,0) &= \psi_1(x,H) = 0 \quad \text{(Quantum Mechanical)} \\ \psi_0(x,h) &= \psi_1(x,h) \\ \frac{1}{\rho(x)}\frac{\partial\psi_0}{\partial z}(x,h) &= \frac{1}{\rho_1}\frac{\partial\psi_1}{\partial z}(x,h) \quad \text{(Acoustic)} \\ \frac{\partial\psi_0}{\partial z}(x,h) &= \frac{\partial\psi_1}{\partial z}(x,h) \quad \text{(Quantum Mechanical).} \end{aligned} \tag{4}$$

Alternatively, we can consider the system to be periodic in z as well as x, in which case we are led to the Floquet condition

$$\psi_0(x,0) = e^{i\beta_z H}\psi_1(x,H). \tag{5}$$

The system then describes a periodic array of grating structures, or doubly periodic one-dimensional nonlinear lenses. This is the most general boundary condition, since linear combinations can be taken to satisfy any of the boundary conditions (4).

The wave equation in each region is separable, and a general solution may be written in the Floquet form

$$\begin{aligned}\psi_1(x,z) &= \sum_n [a_n^+ \exp(ik_n^z(1-z)) + a_n^- \exp(-ik_n^z(1-z))] \exp(ik_n^x x) \\ \psi_2(x,z) &= \sum_m [b_m^+ \exp(i\kappa_m^z z) + b_m^- \exp(-i\kappa_m^z z)] \sum_n V_{mn} \exp(ik_n^x x),\end{aligned} \tag{6}$$

where

$$\begin{aligned}k_n^x &= \beta_x + nK_w, \\ k_n^z &= +[\rho_0 k^2 - (k_n^x)^2]^{\frac{1}{2}} \\ \kappa_m^z &= +[\rho_1 k^2 - (\beta_x + \lambda_m K_w)^2]^{\frac{1}{2}},\end{aligned} \tag{7}$$

β_x is the Bloch wavevector (Floquet multiplier) in the x direction, and λ_m denotes the m^{th} eigenvalue of the Mathieu operator $\hat{M} = d^2/d\theta^2 + (k^2\varepsilon/K_w^2)\cos\theta$. For the quantum mechanical case, we have $\hat{M} = d^2/d\theta^2 + (2m\varepsilon/\hbar^2 K_w^2)\cos\theta$. The associated eigenfunctions are the periodic Mathieu functions [6], with Fourier coefficients V_{mn}. Note that each space harmonic in the uniform region satisfies the wave equation individually, while a solution inside the grating consists of an infinite sum over space harmonics induced by the periodic modulation.

The eigenfrequencies of the system are determined by the matching conditions at the interface, which lead to the requirement that a certain infinite order determinant vanish. It is shown in Appendix A that for acoustic boundary conditions this determinantal condition is given by

$$\det|V_{nm}\left\{\frac{k_n^z}{\rho_1}\tan[k_n^z(1-h)] + \frac{\kappa_m^z}{\rho_0}\tan(\kappa_m^z h)\right\}| = 0. \tag{8}$$

In this equation, the parameters k_n^z, κ_m^z, and the expansion coefficients are all functions of the frequency.

The computation of the spectrum is greatly simplified by a periodicity requirement that is now imposed: acceptable wavefunctions have the periodicity of the

grating, so that $\beta_x = 0$ (the system lies on a cylinder). In other words, the spectrum of interest is at the center of the Brillouin zone. A special case of this requirement is the set of real even or odd periodic solutions: these solutions correspond to creating a physical cavity by putting walls (or conducting surfaces) at $x = \pm\pi/K_w$. The eigenvalues and eigenvectors of the Mathieu equation are obtained using a numerical method due to Hodge [7]. The recursion relations for the Fourier coefficients are reduced to a symmetric, tridiagonal matrix equation which is solved using the bisection method.

C. Spectrum and Eigenmodes

We illustrate qualitative features of the typical system behavior in fig. 2a, where a portion of the frequency spectrum is plotted as a function of the perturbation strength $\varepsilon = \eta\rho_0$. Only even parity modes are shown, as modes of different parity are decoupled. The spectrum of eigenvalues as a function of ε has been determined for $0 < \varepsilon < 0.5$, a range which encompasses the transition from completely regular motion at $\varepsilon = 0$ to globally stochastic motion in the ray system. Eigenvalues have been computed for $k^2 = \omega^2/c_0^2 < 3000$ cm^{-2}, about 80 levels total. Note that k^2 rather than k is plotted , because the eigenvalue density is (asymptotically) uniform in k^2 for a two-dimensional system (the density of modes in k space is $dN = 2\pi k dk$, and $N(k) \propto k^2$. The most striking feature of this plot is the complete absence of degeneracies: eigenvalues approach one another but do not cross. This behavior is expected for a system without symmetry (for given parity) as one parameter is varied; in general one must vary two parameters to produce a degeneracy [8]. One such avoided crossing is illustrated in fig. 2b.

In fig. 3, a part of the same region of the (quantum mechanical) spectrum is shown for two different values of the eikonal parameter $\hbar$. Each plot shows levels for the same set of states, *i.e.*, with the same set of quantum numbers at $\varepsilon = 0$. The square wavenumbers $k^2 = 2E/\hbar^2$ are the same at $\varepsilon = 0$ for each plot, and thus $E(k^2)$ and the level spacings decrease as $\hbar$ decreases. It is apparent that the spectrum grows more sensitive to the perturbation as $\hbar$ decreases, consistent with the observation that

the classical particle dynamics grow more chaotic for lower energy.

The modes of the system may be obtained by solving the linear system (A1) for the expansion coefficients a and b. One interesting feature of the wavefunctions is the intensity distribution in configuration space given by the absolute square. We show in fig. 4 a contour plot of the intensity for a typical even parity wavefunction, symmetric about the center of the waveguide. We observe clear concentration of probability about the stable classical periodic orbit forming a "V" in the waveguide.

III. RAY AND PARTICLE DYNAMICS

A. Waveguide Map

We now consider the ray or particle dynamics associated with the wave equation (2) in the limit $k \to \infty$. Our principal aim is to identify the parameter regimes and initial conditions leading to regular or stochastic motion in phase space. The motion is the composition of two integrable motions: free particle trajectories outside the grating, and a one-dimensional pendulum inside. Therefore it is staightforward to compute the exact dynamics at all times in terms of straight line trajectories (outside) and the Jacobi elliptic functions (inside), joining solutions at the interface such that momentum parallel to the surface is conserved. Thus this system has the desirable feature of admitting an exact Poincaré map without the need to resort to numerical integration or approximations to the dynamics. Ray trajectories for geometrical acoustics or optics are identical to the particle paths if the proper choice of canonical coordinates is made [9]. If ray paths are parametrized by z rather than the time, one may obtain the equations of motion for the canonical variables (x, p) from the nonautonomous Hamiltonian

$$H_{opt}(x, p; z) = -\sqrt{N^2(x, z) - p^2}, \tag{9}$$

where $N(x, z)$ is the density or index of refraction,

$$N^2(x) = \begin{cases} N_0^2\{1+\eta\cos(K_w x)\}, & 0 < z \le h \\ N_1^2, & h < z \le H. \end{cases} \tag{10}$$

This Hamiltonian may be obtained by extracting a Lagrangian from Fermat's action principle and making a Legendre transformation [9]. The momentum p is the acoustical or optical direction cosine of the ray:

$$p = N(x,z)\sin\alpha = N(x,z)\frac{k_x}{|k|} \tag{11}$$

where α is the angle the ray makes with the z axis.

If $N^2(x)$ is written in the form

$$N^2(x,z) = N_0^2 - \delta N(x,z), \tag{12}$$

then equation (9) is equivalent to

$$H_{cl} = P_x^2 + P_z^2 + \delta N^2(x,z) = N_0^2, \tag{13}$$

where we have identified $H_{opt} = -P_z$ and $p = P_x$, the Cartesian momenta. Therefore the ray trajectories in a medium of index of refraction $N(x,z)$ are identical to particle trajectories in a potential $V(x,z) = \delta N^2(x,z)$. The constant N_0^2 plays the role of the numerical value of the Hamiltonian.

The relevant particle or ray Hamiltonian for the waveguide is thus

$$H_{cl}(x,z,P_x,P_z) = \tfrac{1}{2}(P_x^2 + P_z^2) + V(x,z), \tag{14}$$

with

$$V(x,z) = \begin{cases} \infty, & z \le 0 \text{ or } z \ge H; \\ V_0 = \text{const}, & h \le z < H; \\ -\varepsilon\cos(K_w x), & 0 < z \le h. \end{cases} \tag{15}$$

The perturbation strength ε for an optical ray system is $\varepsilon = \eta N_0^2$; for a particle system it is just the potential strength. Defining the wall phase $\theta = K_w x$, and taking $p = P_x$, a surface of section is chosen such that the pair (θ, p) are determined just before the

particle strikes the upper wall at $z = H$; P_z is then fixed by energy conservation. With this choice, the dynamics may be expressed as the composition of three area preserving maps, taking the particle 1) from the upper wall to the grating surface; 2) from the grating surface until it re-exits; 3) from the grating surface back to the upper wall (fig. 5). These maps may be written explicitly as follows:

$$\begin{aligned}
&1.\ \theta_2 = \theta_1 + k_w H \frac{p_1}{\sqrt{2(E - \frac{1}{2}p_1^2)}} \\
&\quad p_2 = p_1 \\
&2.\ \theta_3 = \Theta(\theta_2, p_2) \\
&\quad p_3 = \mathcal{P}(\theta_2, p_2) \\
&3.\ \theta_4 = \theta_3 + k_w H \frac{p_3}{\sqrt{2(E - \frac{1}{2}p_3^2)}} \\
&\quad p_4 = p_3
\end{aligned} \tag{16}$$

The functions $\Theta, \mathcal{P}$ in step 2, representing the exact dynamics within the layer, may be given in terms of the Jacobi elliptic functions sn, cn, and dn [6] as follows:

$$\Theta(\theta, p) = \begin{cases} 2\arcsin[K\mathrm{sn}(\omega_0 t + \phi, K)], & K^2 < 1 \\ 2\arcsin[\mathrm{sn}(K\omega_0 t + \phi, 1/K)] & K^2 \geq 1 \end{cases} \tag{17}$$

$$\mathcal{P}(\theta, p) = \begin{cases} 2\omega_0 K/K_w \mathrm{cn}(\omega_0 t + \phi, K) & K^2 < 1 \\ 2\omega_0 K/K_w \mathrm{dn}(K\omega_0 t + \phi, 1/K) & K^2 \geq 1 \end{cases} \tag{18}$$

where

$$\begin{aligned}
K^2 &= \tfrac{1}{2}\left(\frac{p^2}{2\varepsilon} + 1 - \cos\theta\right) \\
\omega_0 &= K_w\sqrt{\varepsilon} \\
t &= \frac{\sqrt{2}h}{[E - \frac{1}{2}p^2 + \varepsilon\cos\theta]^{\frac{1}{2}}}
\end{aligned} \tag{19}$$

and $\phi = \phi(\theta, p)$ is chosen to conform to the initial conditions, *i.e.* $(\Theta, \mathcal{P})_{t=0} = (\theta, p)$. We choose to write the mapping in this three step symmetric form because the surface of section plot then has both reflection (about $\theta = 0$) and inversion symmetry.

B. Fixed Points and Linear Stability

The period one fixed points are determined by setting $\theta_4 = \theta_1$, $p_4 = p_1$. This implies

$$\mathcal{P}(\theta_2, p_1) = p_1 \tag{20}$$

with θ_2 defined above. By simple geometry one obtains two such points θ^n as

$$\theta^n = n\pi, \quad n = 0, 1 \tag{21}$$

Thus the pair (θ^n, p^n) are determined by solving the transcendental equation

$$p^n = \mathcal{P}\Big(n\pi + k_w H \frac{p^n}{\sqrt{2(E - \frac{1}{2}(p^n)^2)}}, p^n\Big) \tag{22}$$

for p^n. The stability of the central resonance $n = 0$ at $(0, 0)$ is of interest because it is the last to go unstable as ε is increased. The Jacobian matrix M of the mapping at this point can be shown to be

$$\mathrm{M} = \begin{pmatrix} \cos(\omega t) - C\sqrt{\varepsilon}\sin(\omega t) & -\sqrt{\varepsilon}\sin(\omega t) \\ (1/\sqrt{\varepsilon} - \sqrt{\varepsilon}C^2)\sin(\omega t) + 2\cos(\omega t) & \cos(\omega t) - C\sqrt{\varepsilon}\sin(\omega t) \end{pmatrix}, \tag{23}$$

where $C \equiv K_w H/\sqrt{2}$. Stability requires $\mathrm{Tr}\mathrm{M} < 2$ [5]; in this case

$$\sqrt{\varepsilon} C \sin(\omega t) - \cos(\omega t) < 1 \tag{24}$$

The stability border is then explicitly determined by

$$K_w H \sqrt{\varepsilon/2} \tan\Big\{K_w h \sqrt{\frac{\varepsilon}{2(E+\varepsilon)}}\Big\} = 1. \tag{25}$$

Surface of section plots are shown in fig. 6. The horizontal axis displays the wall phase $\theta = K_w x$, which is periodic with period 2π; the vertical axis shows $p/\sqrt{2E}$. For

these plots, the parameters K_w, h, and H are fixed while ε is varied. At the chosen values, $K_w = 10$, $h = 0.1$, $H = 1$, and $E = 1$, the central fixed point goes unstable at $\varepsilon \approx .239$, according to equation (21). This is borne out numerically, as we witness a period-doubling bifurcation at this value of ε. A notable feature of this map is the presence of 'trapped' orbits, where the particle is temporarily confined to the grating or uniform region because P_x is too small for penetration to occur. For such an orbit, specular reflection occurs until the potential is small enough to admit the particle to the grating. A particle confined to the uniform region in this manner will conserve P_x, hence the map will display consecutive points on a line P_x=constant before re-entry occurs. Thus a stochastic orbit can appear regular for several iterations. Note also that stochasticity always exists near grazing incidence of the ray even for small ε. This is due to many overlapping resonances, which grow arbitrarily close in momentum space near $P_x = 1$. We have also explored the behavior of the mapping as the energy is varied. Because the interaction of the particle with the layer is greater for smaller energy, the stochasticity present increases with decreasing energy.

C. Relation to the Standard Mapping

Near normal incidence, the mapping (16) is well approximated by the well known standard mapping, provided the x coordinate of the particle changes little within the layer. Since the magnitude of the force experienced by the particle within the layer is $F_x \sim \varepsilon K_w$, and the interaction time is $t = h/P_z \approx h/\sqrt{E+\varepsilon}$, we require

$$F_x t^2 = \varepsilon \frac{K_w^2 h^2}{\sqrt{E+\varepsilon}} \ll 1. \tag{26}$$

Then taking $\Delta p = Ft$ as the impulse received at each encounter with the layer, the mapping immediately follows as

$$\begin{aligned} I_{n+1} &= I_n + K_{cl} \sin\theta_n \\ \theta_{n+1} &= \theta_n + I_{n+1}, \end{aligned} \tag{27}$$

where

$$I \equiv \frac{2K_w H}{\sqrt{E+\varepsilon}} p$$

and

$$K_s = \frac{2\varepsilon K_w^2 Hh}{E+\varepsilon}. \tag{28}$$

This is just Chirikov's standard mapping with stochasticity parameter K_{cl} [5]. If in addition we have $\varepsilon \ll 1$, then

$$K_{cl} \approx 2(\frac{\varepsilon}{E})(K_w h)(K_w H), \tag{29}$$

revealing its dependence on the dimensionless perturbation strength and scale lengths. Observe that the stability border given by equation (25) is simply a condition on the standard map K_{cl} in the limit considered here.

Equation (28) or (29) provides a criterion for the transition to global stochasticity in this system, which occurs in the standard mapping at $K_{cl} \approx 1$. Although the standard mapping is only a local approximation derived here for the central resonance, we note that this criterion should provide at least an upper bound; the separation of period one islands decreases with increasing action, accumulating at $p = 1$, so that the phase plane has a larger measure of stochastic orbits than the standard map approximation.

IV. THE WAVE MAPPING

In the regime where the standard mapping is a good approximation to the dynamics, the paraxial wave equation is also a valid approximation. The paraxial description allows us to view the wave dynamics in the context of an initial value problem at fixed frequency; it is useful for guided beam systems such as optical fibers [10]. In this section it is convenient to adopt the interpretation of our system as a guiding structure loaded with a periodic array of nonlinear lenses as in equation (5), although the results will also apply to waves near normal incidence in the cavity described by (8). The essential required feature for this section is that the spectrum of transverse modes for the guiding structure be discrete and not continuous.

The paraxial approximation consists in taking $p^2 \ll N^2$ in equation (9), so that

$$H_{opt}(x,p;z) \approx \frac{p^2}{2N(x,z)} - N(x,z). \tag{30}$$

From the point of view of the wave operators $\mathbf{k} \to -i\nabla$, this makes the associated wave equation first order in z. Alternatively, we can make the substitution [10]

$$\psi(x;z) = \Phi(x;z)\exp(ikz) \tag{31}$$

in the wave equation (2), and neglect second derivatives with respect to z. The resulting paraxial wave equation is

$$-\frac{i}{k}\frac{\partial \Phi}{\partial z}(x;z) = -\frac{1}{2N_0 k}\frac{\partial^2 \Phi}{\partial x^2}(x;z) + \eta N_0 \cos(K_w x)[\Theta(z) - \Theta(z-h)]\Phi(x;z), \tag{32}$$

where $\Theta(z)$ denotes the unit step function. We remark that the parabolic wave equation derived in this manner is not unique, but represents a particular choice of approximation to the square root operator embodied in equation (9). This issue is discussed in refs. 11 and 12. Equation (32) is just the Schrödinger equation with the z-dependent potential

$$V(x;z) = \eta N_0 \cos(K_w x)[\Theta(z) - \Theta(z-h)], \tag{33}$$

and eikonal parameter k in the role of $\hbar$. Within this framework, a mapping for the wavefield Φ may be derived for the system. The procedure is similar to the elliptic case: we solve the wave equation in each region, and match solutions (but not z derivatives) at the interface. The mapping so obtained is

$$a_n^{N+1} = \sum_{mn'} V_{mn} V_{mn'} a_{n'}^N \exp(i[1-h]k_{n'}) \exp(i\kappa_m h), \tag{34}$$

where

$$k_{n'} = k - \frac{(k_{n'}^x)^2}{2k}$$

and

$$\kappa_m = k - \frac{(\beta_x + \lambda_m K_w)^2}{2k}.$$

If we take the thin lens limit $h \to 0$ and $N_0 \to \infty$, holding fixed the optical length $h_{opt} = N_0 h$, the potential (33) becomes

$$V(x,z) = \eta h_{opt} \cos(K_w x)\delta(z - H). \tag{35}$$

The ray mapping corresponding to this potential is just the standard mapping with stochasticity parameter $\eta K_w^2 H h_{opt}$. It can be shown that in this limit the wave mapping (34) reduces to

$$a_n^{N+1} = \sum_m (i)^{(n-m)} J_{n-m}(\epsilon) \exp(-im^2\tau/2 + i\phi) a_m^N, \tag{36}$$

where $\epsilon = \eta k h_{opt}$, $\tau = K_w^2 H/k$, and $\phi = k(H + h_{opt})$; $J_\nu(\epsilon)$ denotes the Bessel function of the first kind of order ν.

We also remark here on the relation between this problem and a different kind of boundary perturbation. Frequently it may be desirable to replace the periodic grating of varying dielectric constant ϵ with one of modulated height and constant ϵ. Then by applying the appropriate boundary conditions at the interface, one arrives at a paraxial mapping

$$a_n^{N+1} = \sum_m \exp(i[k_n^0(H - h) + k_n^1 h]) J_{n-m}(k_n^0 \eta h) J_{m-n}(k_m^1 h) a_m^N, \tag{37}$$

where $k_n^\alpha = N_\alpha k - n^2 K_w^2 / N_\alpha k$, N_α is the index of refraction for the region α, h and H are the (unmodulated) heights of each region, and η is the modulation depth in units of h. The Fresnel limit consists in taking $h \to 0$ and $N_0 \to \infty$, holding fixed $h_{opt} = N_0 h$ as before. The result is the wave mapping

$$a_n^{N+1} = \sum_m \exp(ik_m^1 H) \exp(ikh_{opt}) J_{n-m}(kh_{opt}) a_m^N, \tag{38}$$

which is the same as (36) with $N_1 = 1$.

The wave mapping (36) or (38) is identical in form to the much studied quantum standard mapping [13]. The wavefield defined by the as is localized in k_x space, for $\tau/2\pi$ a generic irrational number [14]; the eigenvectors of the unitary transformation defined in (36) are concentrated about a particular wavevector site $k_n^x = nK_w$ and decay away from that site with a characteristic decay length δk_x, the *localization*

length. By Floquet's theorem, the associated eigenvalues are of the form $\exp(i\omega_\alpha)$; the *quasienergies* ω_α form a discrete set. In the stochastic regime $K_{cl} \gg 1$, which corresponds to an unstable optical ray, the localization length δk_x scales as $\delta k_x \sim \epsilon^2 \tau K_w$ [15,16]. Using the definitions of ϵ and τ given previously, we have $\delta k_x \sim \eta^2 K_w^2 k h^2 H$. This quantity diverges as $1/\lambda$ in the eikonal limit ($k \to \infty$), as expected for unstable rays. In practical situations, the effect of localization is important only if δk_x is smaller than some wavevector scale length in the problem. In addition, for the present situation a large localization length is inconsistent with the paraxial assumption which requires $\delta k_x / k \ll 1$. Therefore we are led to ask if there exists a parameter regime of interest for which (1) rays are unstable, (2) localization is predicted in k_x space, and (3) the paraxial assumption is valid.

The answer is yes. The ray instability border is determined by

$$\eta K_w^2 H h = K_{cl} \approx 1, \tag{39}$$

while the localization spread $\delta k_x / k \sim \eta^2 K_w^3 h_{opt}^2 H$. Note that the fractional spread in the wavevector is independent of k. Requiring the condition $\delta k_x / k \ll 1$ for $K_{cl} \ll 1$, we obtain

$$\eta K_w h_{opt} \ll 1. \tag{40}$$

Furthermore, the ray treatment is sensible only if $k \gg K_w$. Therefore we are led to the ordering

$$K_w h_{opt} \ll \frac{1}{\eta} \ll K_w H \tag{41}$$

for these three conditions to be valid. Equation (39) also implies $K_w H \gg 1$. These inequalities are easily satisfied for optical systems of interest.

One is naturally led to ask what wavevector localization implies for the configuration space wavefunction, whose square is the intensity profile of an optical beam. To study this, we evolve a Gaussian wavepacket well localized in configuration space, as in a beam. For an initial state localized about $(k_x, \theta) = (0, 0)$, we find that for $K_{cl} = 4.0$ the state spreads somewhat in θ but remains clearly localized about the initial phase point (see fig. 7a). This might be expected based on the persistence of

the primary island for this value of K_d. However, at a value of K_d well above the bifurcation value for the primary island, we still observe spatial localization, in contrast to the classically expected result. In addition, we have observed that a wave packet initially localized outside the primary island at $K_d = 4$ also remains concentrated about its initial condition. We show in fig. 7b and 7c an example of localization persisting at $K_d = 5$, when the classical phase space is globally chaotic. We conclude that a Gaussian beam in this lens system will remain concentrated about the optical axis if it is initially so, even in the regime of strong ray stochasticity.

As K_d increases at fixed ϵ, the configuration space intensity remains nonuniform, although the density is not always concentrated at the initial point $\theta = 0$. This is presumably due to fluctuations in phase and amplitude in the k_x space wavefunction, although the envelope remains roughly constant. We illustrate this behavior in fig. 7d.

One might imagine that the phase error inherent in the paraxial approximation could invalidate our results. Thus we comment here on the importance of higher order terms in the paraxial expansion (30) of the optical Hamiltonian. Localization results as a consequence of the pseudorandomness of the sequence $T_n = \tan(k_n H)$, where

$$\begin{aligned} k_n H = (k^2 - n^2 K_w^2)^{\frac{1}{2}} H &= k - n^2 K_w^2 H/2k + n^4 K_w^4 H/8k^3 + \dots \\ &= kH - n^2 \frac{\tau}{2} + n^4 \frac{\tau^2}{8kH} + \dots \end{aligned} \tag{42}$$

Since we only require $n^2 K_w^2/k^2 \ll 1$ and $n^2 K_w^2/k \gg 1$ for paraxial behavior and pseudorandomness respectively, the third term in the expansion may be comparable to 2π and introduce significant phase error. However, the conclusions based on (36) remain valid because the sequence T_n is *still* a pseudorandom one. In fact, the effect of the higher order terms could serve to "soften" quantum resonances which occur at rational values of $\tau/4\pi$ [17]. We illustrate this effect in Fig. 8, where we set $\tau = \pi/2$ and $kH = 100$, so the third term in (42) is $k_n^{(3)} \approx .003n^4$. The solid lines show the results of including the higher order n^4 term, whereas the dotted lines include only the n^2 term. In Fig. 9a, we contrast the resonant k space density distribution ρ with the clearly exponentially localized solid line. Fig. 9b shows the spread of the distributions with time: the additional term completely destroys the resonant absorption in mean

square wavenumber. These results are easily understood in terms of the unperturbed ($\epsilon = 0$) quasienergy spectrum, which consists of levels with unequal spacings due to the fourth order term in the expansion of the optical Hamiltonian. Since the spacings are unequal, a resonant excitation at a frequency equal to a transition frequency in the system will eventually detune from resonance. Equivalently, at resonance the unperturbed quasienergy spectrum consists of a finite number of levels equally spaced on the unit circle; the higher order terms destroy this structure and give instead an infinite number of levelsuniformly distributed on the circle. Interestingly, the same modification to the classical standard mapping destroys the classical anologue to quantum resonance, the accelerator modes.

V. SUMMARY AND CONCLUSIONS

We have demonstrated the relevance of wavevector and spatial localization to a class of systems with a variety of physical applications. To accomplish this, we have examined three aspects of a waveguide system, which is described in the eikonal limit by a ray system having near-integrable dynamics. First, we gave a qualitative picture of the solutions to the time-independent Helmholtz equation in the system. Second, the exact ray dynamics were obtained and described by phase portraits, and the degree of system stochasticity was determined as a function of perturbation strength. A simple mapping approximating the exact surface of section mapping was derived. Third, a wave mapping for the system was obtained valid in the paraxial regime. Localization in wavevector space was seen to emerge as a consequence of the paraxial unitary wave propagator, which is closely related to the quantum standard mapping. Since the quasieigenmodes of the wave mapping are approximate solutions to the time independent Helmholtz equation for the waveguide, the localized nature of the solutions reveal qualitative information about the eigenstates of the original system.

The validity of our results is confirmed by considering their sensitivity to the model assumptions. Because the eigenmodes are found to be localized in k_x space,

the validity of the paraxial approximation ($k_x \ll k$) is confirmed, even in the regime of strong ray stochasticity. We have also established that the phase error inherent in the paraxial approximation does not invalidate localization, but rather contributes to the disorder which produces it. The remaining assumption of unitarity is violated due to reflected waves at the focusing elements, which will be small provided the modulation strength η is small compared to unity.

Finally, we remark that the results *do* depend strongly on the boundary conditions taken, as suggested at the beginning of section IV. In particular, if we had allowed a continuous spectrum for the transverse wavevector β_x (by removing the boundary), then the unperturbed system would have a continuous spectrum and localization would not occur [18]. For the guided lens waveguide and cavity systems considered above, the boundary conditions and a discrete unperturbed spectrum are natural.

This work was supported by National Science Foundation Grant ECS-8517364 and Office of Naval Research Contract N00014-84-K-0367.

APPENDIX A

The determinant (8) yielding the eigenfrequencies is obtained byrequiring the wave functions (6) to satisfy the boundary conditions (4) at the grating surface $z = h$. Substituting from equations (6) into equations (4), one obtains

$$\sum_n a_n \cos[k_n^z(1-h)] \exp(ik_n^x x) = \sum_m b_m \cos(\kappa_m^z h) \sum_n V_{mn} \exp(ik_n^x x)$$
$$\frac{1}{\rho_1} \sum_n a_n k_n^z \sin[k_n^z(1-h)] \exp(ik_n^x x) = -\frac{1}{\rho_0} \sum_m b_m \kappa_m^z \sin(\kappa_m^z h) \sum_n V_{mn} \exp(ik_n^x x), \tag{A1}$$

where we have made the simplifying assumption of replacing $\rho(x)$ with ρ_0, so that the velocity is continuous to zero order in η. The condition that the coefficients of $\exp(ik_n^x x)$ vanish separately is therefore, in matrix form:

$$\begin{aligned} \mathbf{A_1 b} - \mathbf{B_1 a} &= \mathbf{0} \\ \mathbf{A_2 b} + \mathbf{B_2 a} &= \mathbf{0} \end{aligned} \tag{A2}$$

where

$$[\mathbf{A_1}]_{mn} = \cos(\kappa_m^z h) V_{mn}$$
$$[\mathbf{B_1}]_{mn} = \cos[k_n^z(1-h)] \delta_{mn}$$
$$[\mathbf{A_2}]_{mn} = \kappa_m^z \sin(\kappa_m^z h) V_{mn}$$
$$[\mathbf{B_2}]_{mn} = k_n^z \sin[k_n^z(1-h)] \delta_{mn}$$

These two matrix equations may be combined to yield

$$(\mathbf{B_2 A_1} - \mathbf{B_1 A_2})\mathbf{b} = \mathbf{0} \tag{A3}$$

which will have non-trivial solutions if

$$\det|\mathbf{B_2 A_1} - \mathbf{B_1 A_2}| = 0. \tag{A4}$$

After trivial manipulation the determinental condition may then be given compactly by

$$\det|V_{nm}\{\frac{k_n^z}{\rho_1} \tan(k_n^z(1-h) + \frac{\kappa_m^z}{\rho_0} \tan(\kappa_m^z h)\}| = 0, \tag{A5}$$

as in equation (8). In practice, this determinant requires careful choice of rows and columns to ensure convergence of the Newton root-finding routine used.

References

[1] S. W. McDonald, Ph.D. dissertation, Department of Physics, University of California, Berkeley, CA (LBL report No. LBL-14837) (1983).

[2] S. T. Peng, T. Tamir, and H. L. Bertoni, *IEEE Trans. Microwave Theory and Techniques*, Vol. **MTT-23**, 123 (1975).

[3] C. Elachi, "Waves in Active and Passive Periodic Structures: A Review", *Proc. IEEE*, Vol. 4, 1666 (1976).

[4] J. Z. Wilcox, K. H. Yen, T. J. Wilcox, and G. Evans, *J. Appl. Phys.* **53**, 2862 (1982).

[5] A. J. Lichtenberg and M. A. Lieberman, *Regular and Stochastic Motion*, Springer-Verlag, New York (1983).

[6] M. Abromowitz and I. A. Stegun, *Handbook of Mathematical Functions*, Dover, New York (1965).

[7] D. B. Hodge, "The Calculation of the Eigenvalues and Eigenfunctions of Mathieu's Equation", NASA Contractor Report 1937 (1972).

[8] V. I. Arnold, *Mathematical Methods of Classical Mechanics*, Springer-Verlag, New York, pp. 425-437 (1978).

[9] D. Marcuse, *Light Transmission Optics*, 2nd edition, Van Nostrand Neinhold, New York, p. 94 (1982).

[10] W. K. Kahn and S. Yang, "Application of Hamiltonian Methods to Analogous problems in Optics: Optical Fibers", in *Applications of Mathematics in Modern Optics*, SPIE Vol. 358. (1982)

[11] M. D. Feit and J. A. Fleck, Jr., *J. Opt. Soc. Am.* **B5**, 633 (1988).

[12] D. J. Thomson and N. R. Chapman, *J. Acoust. Soc. Am.* **74**, 1848 (1983).

[13] G. Casati, B. V. Chirikov, F. M. Israilev, and J. Ford, in G. Casati and J. Ford, (eds.), *Stochastic Behavior in Classical and Quantum Hamiltonian Systems*, Lect. Notes in Physics, Vol. 93, Springer-Verlag, New York, p. 334 (1979).

[14] S. Fishman, D. R. Grempel, and R. E. Prange, *Phys. Rev. Lett.* **48**, 509 (1982).

[15] D. L. Shepalyansky, *Physica* **8D**, 208 (1983).

[16] D. L. Shepalyansky, *Physica* **28D**, 103 (1988).

[17] F. M. Izrailev and D. L. Shepalyansky, *Sov. Phys. Dokl.* **24**, 996 (1979).

[18] T. Yukawa, "Semiclassical Limit of the Periodically Kicked Rotator", KEK-Preprint-87-145 (1988).

Figure Captions

Figure 1. A cross sectional view of one period of the periodic waveguide structure.

Figure 2. (a) The eigenvalue spectrum of equation (2) as a function of perturbation strength ϵ, for the range $0 < \epsilon < 0.5$ and $2500\ \text{cm}^{-2} < k^2 < 3045\ \text{cm}^{-2}$. Other parameters are fixed at $K_w = 10\text{cm}$, $H = 1\text{cm}$, $h = 0.1\text{cm}$; the parity is even. (b) A blow up of the boxed region in fig. 2, showing a typical avoided crossing.

Figure 3. The quantum mechanical energy spectrum for $2700\ \text{cm}^{-2} < k^2 < 3050\ \text{cm}^{-2}$, $0 < \epsilon < 0.5$ and two values of $\hbar$: (a) $\hbar = .04$; (b) $\hbar = .01$.

Figure 4. The quantum mechanical probability distribution for $E = 4.4 \times 10^5$, $\epsilon = 0.1$, and $\hbar = .040$.

Figure 5. A ray or particle trajectory in the waveguide, showing the location of the surface of section and the variables appearing in equation (16).

Figure 6. Surface of section plots for the waveguide map (16); 25 initial conditions are iterated 500 times. The parameters are $K_w = 10$, $H = 1$, $h = 0.1$, $E = 1$, and (a)$\epsilon = .05$; (b)$\epsilon = 0.1$.

Figure 7. The asymptotic time averaged intensity and k space density distributions for evolution under the mapping (36); the dotted lines indicate the initial distribution. The parameters are: (a) $\epsilon = 4.0$ and $\tau = 1.0$ ($K_{cl} = 4.0$); (b) $\epsilon = 5.0$ and $\tau = 1.0$ ($K_{cl} = 5.0$); (c) $\epsilon = 50.0$ and $\tau = 0.1$ ($K_{cl} = 5.0$); (d) $\epsilon = 5.0$ and $\tau = 2.0$ ($K_{cl} = 10.0$).

Figure 8. The effect of higher order terms on resonance, for $\tau = \pi/2$ and $kH = 100$: (a) k space density; (b) $\langle k^2 \rangle$ vs. iteration number.

Waveguide Geometry

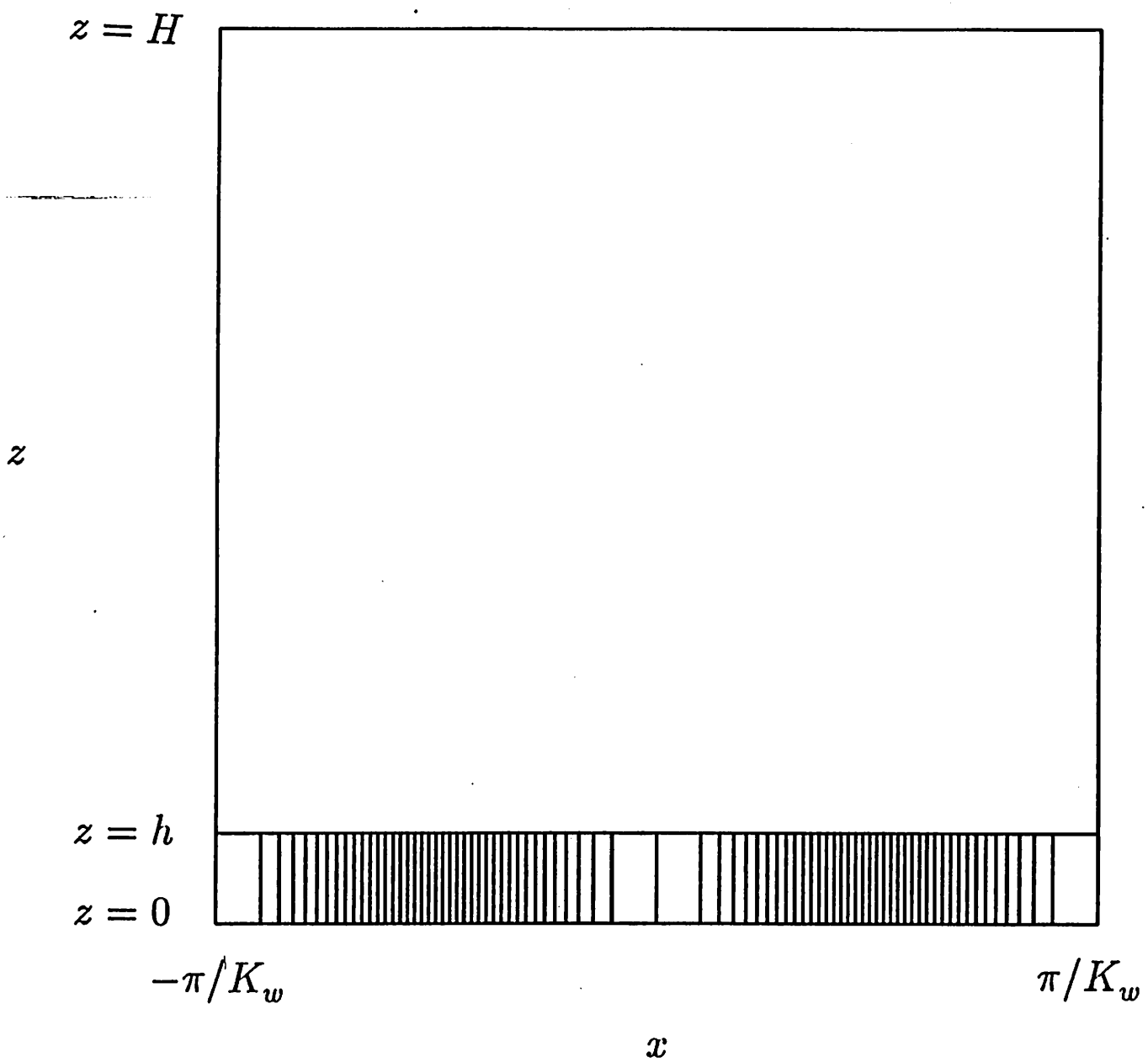

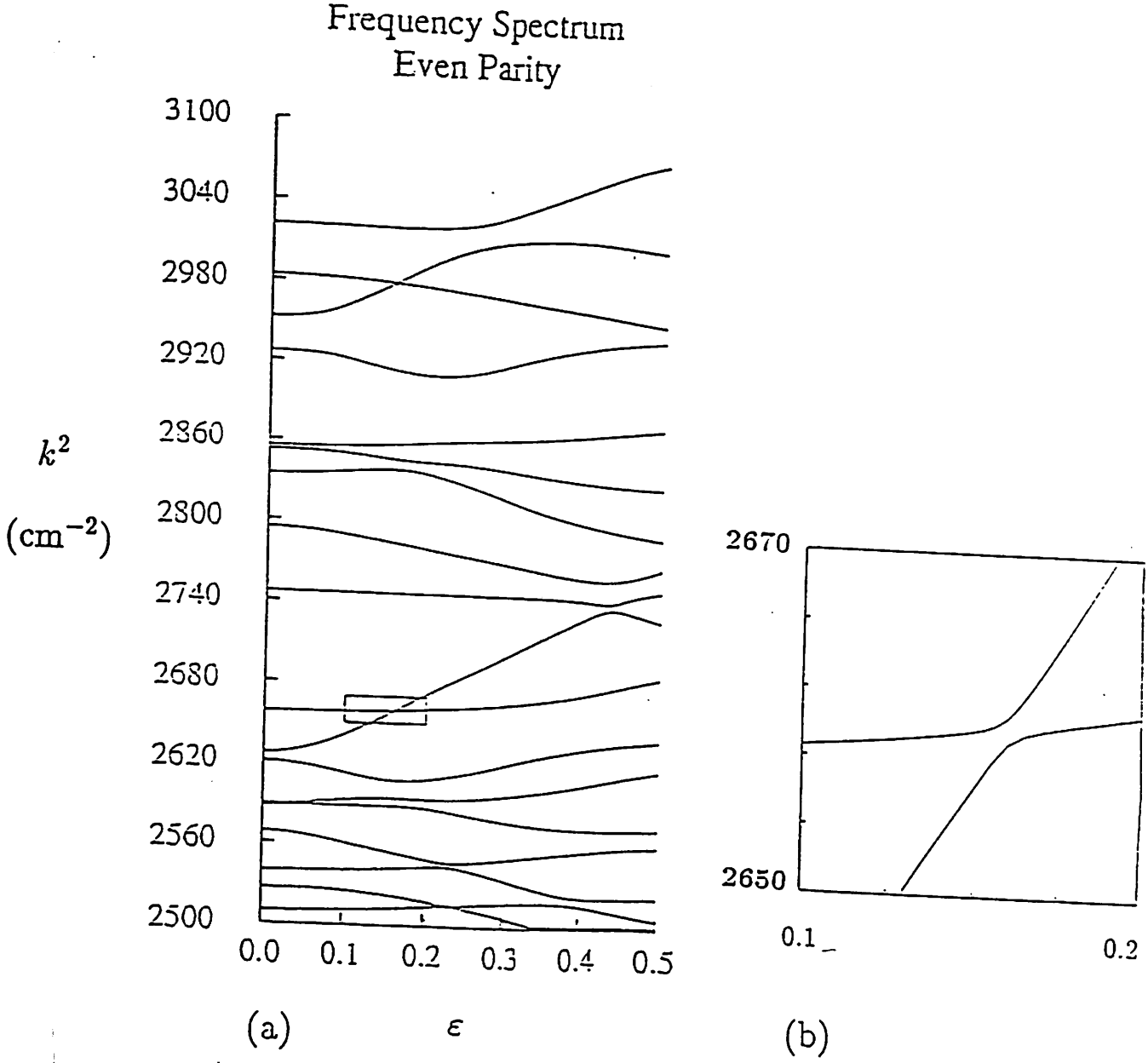
Frequency Spectrum
Even Parity
3100
3040
2980
2920
2860
2800
2740
2680
2620
2560
2500
k^2
(cm^{-2})
0.0
0.1
0.2
0.3
0.4
0.5
ε
(a)
2670
2650
0.1
0.2
(b)

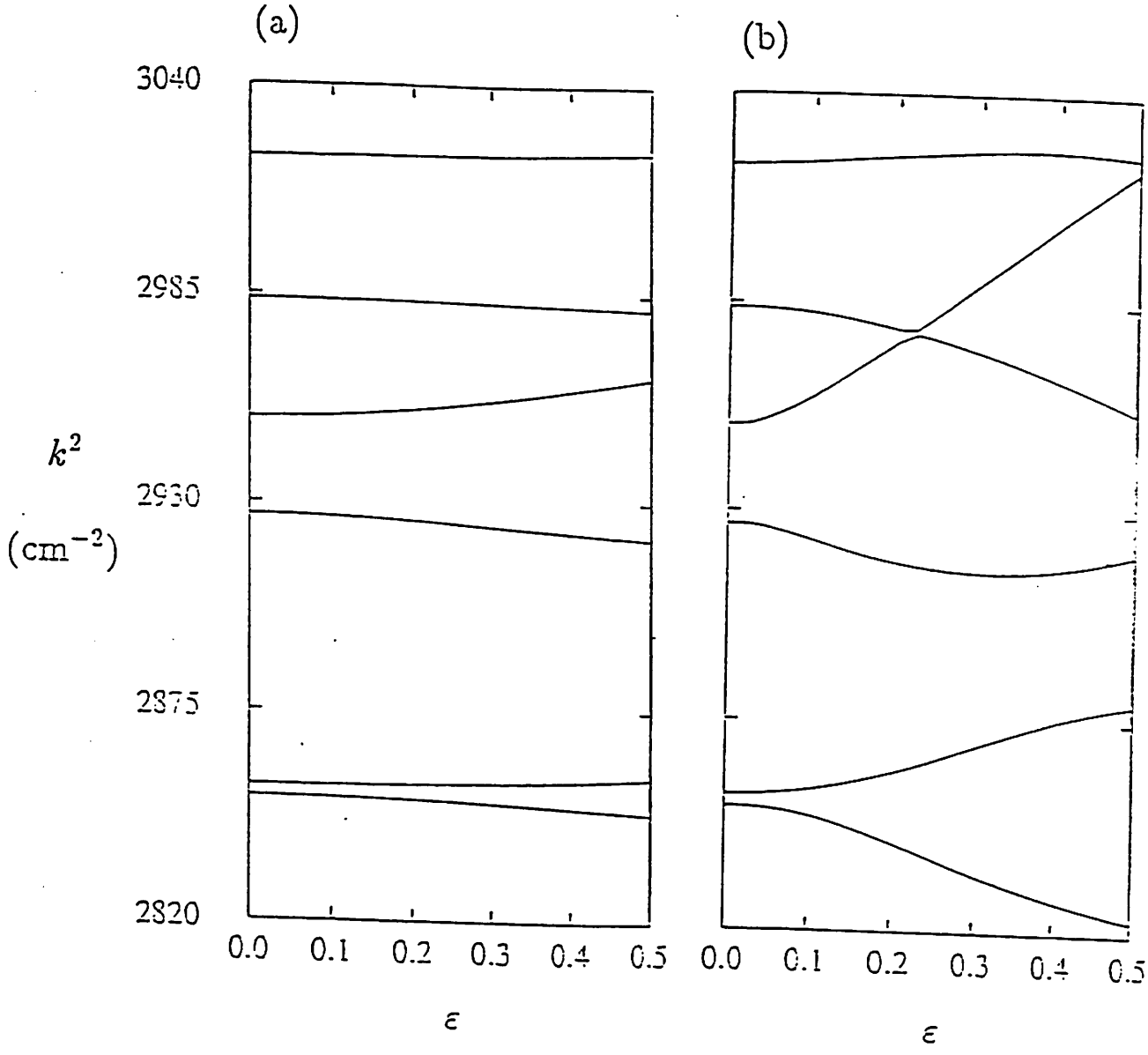
(a)
(b)
3040
2985
2930
2875
2820
k^2
(cm^{-2})
0.0
0.1
0.2
0.3
0.4
0.5
ε

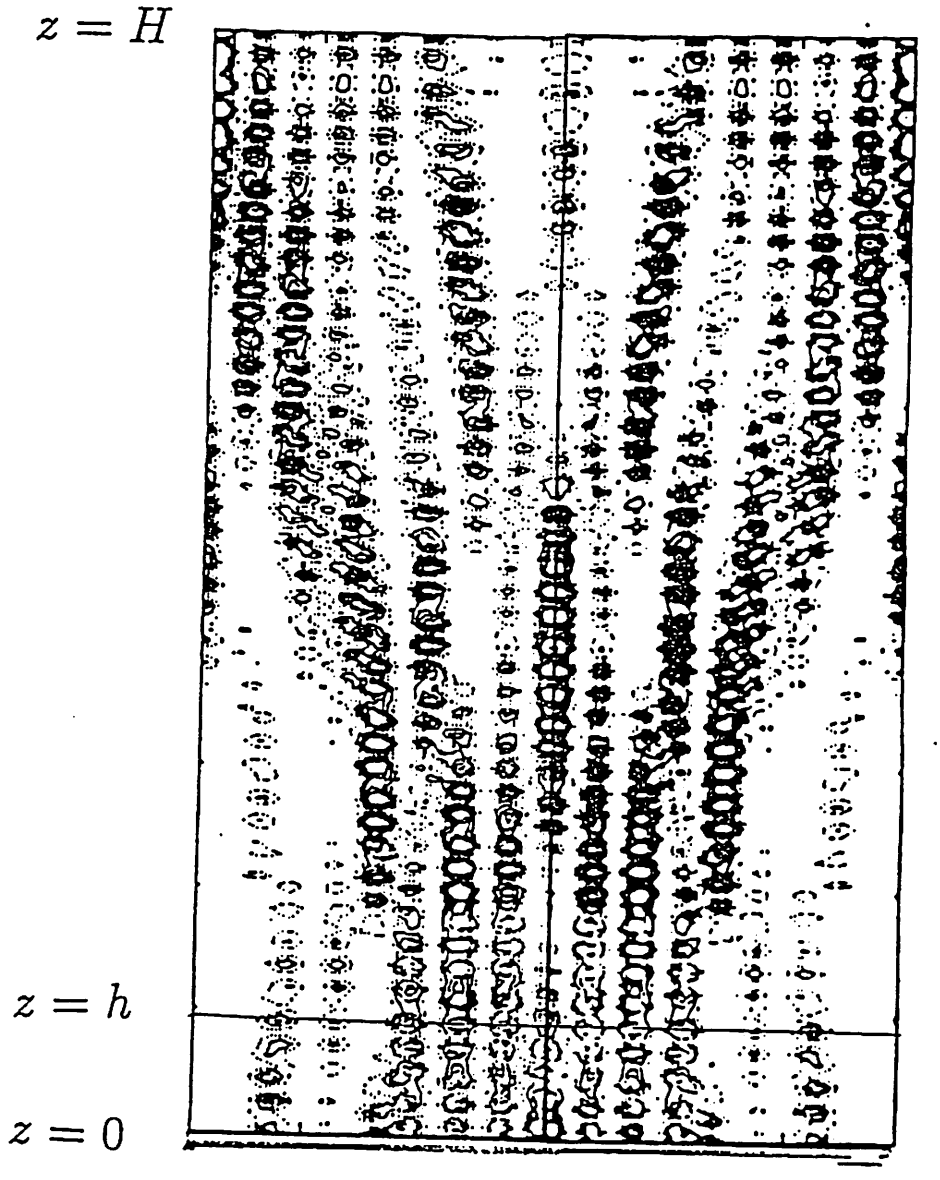
$z = H$
z
$z = h$
$z = 0$
x

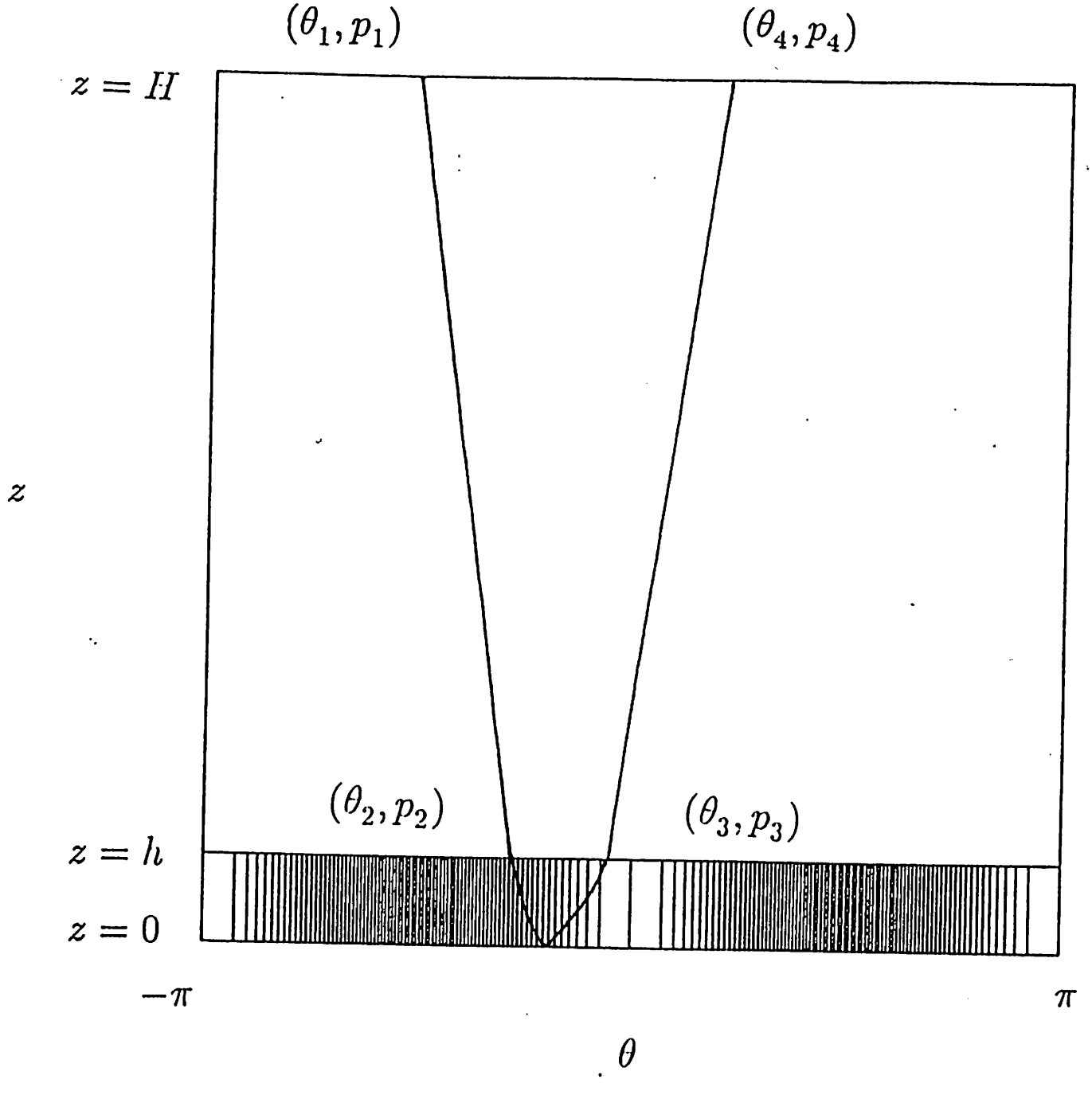
(θ_1, p_1)
(θ_4, p_4)
$z = H$
z
(θ_2, p_2)
(θ_3, p_3)
$z = h$
$z = 0$
$-\pi$
π
θ

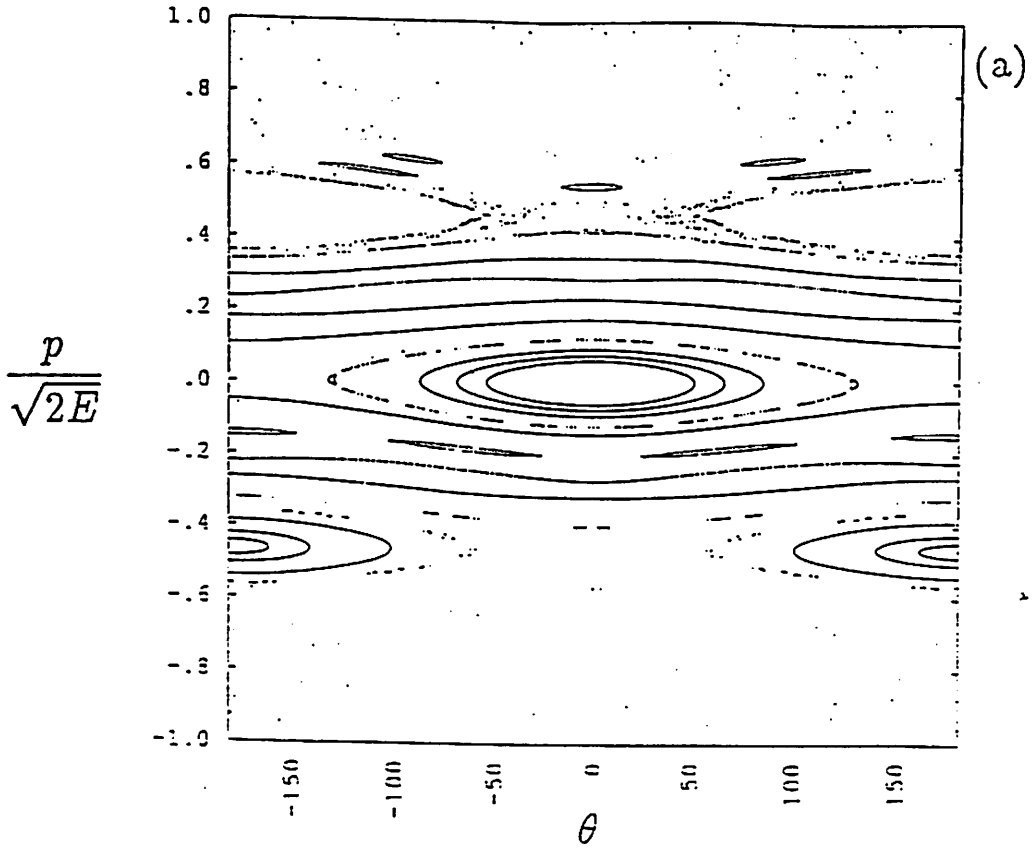
(a)
$\frac{p}{\sqrt{2E}}$
1.0
.8
.6
.4
.2
.0
-.2
-.4
-.6
-.8
-1.0
-150
-100
-50
0
50
100
150
θ

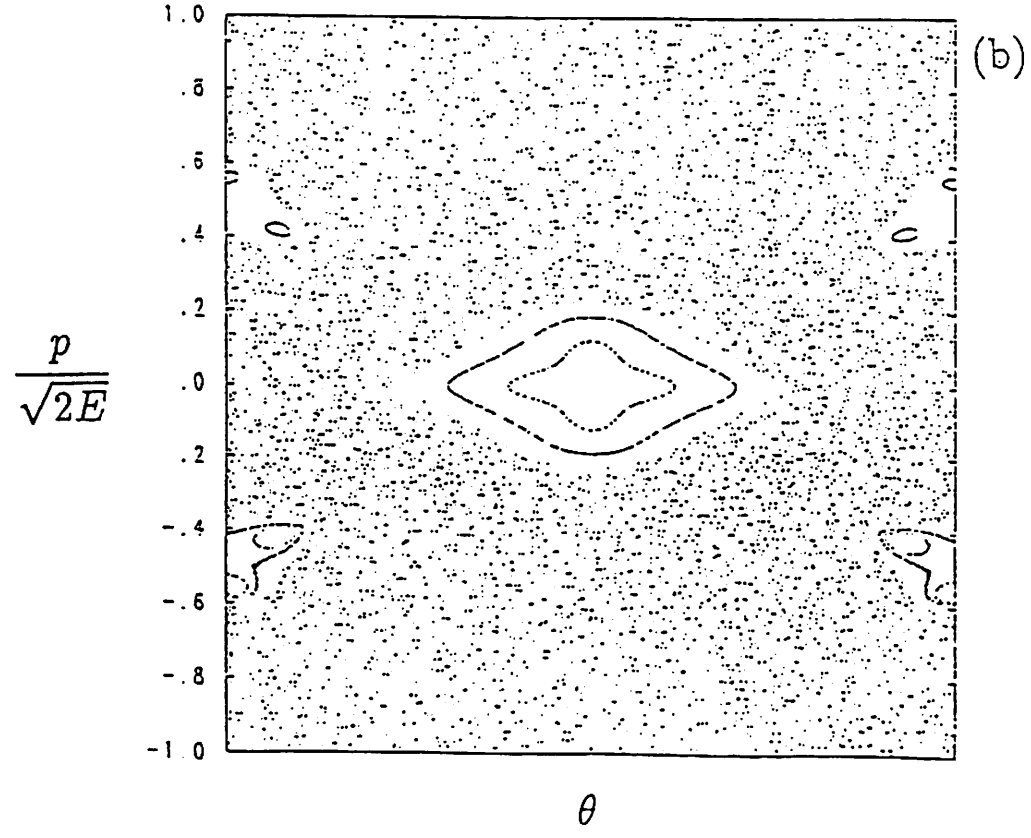
(b)
$\frac{p}{\sqrt{2E}}$
1.0
.8
.6
.4
.2
.0
.2
-.4
-.6
-.8
-1.0
θ

(a)

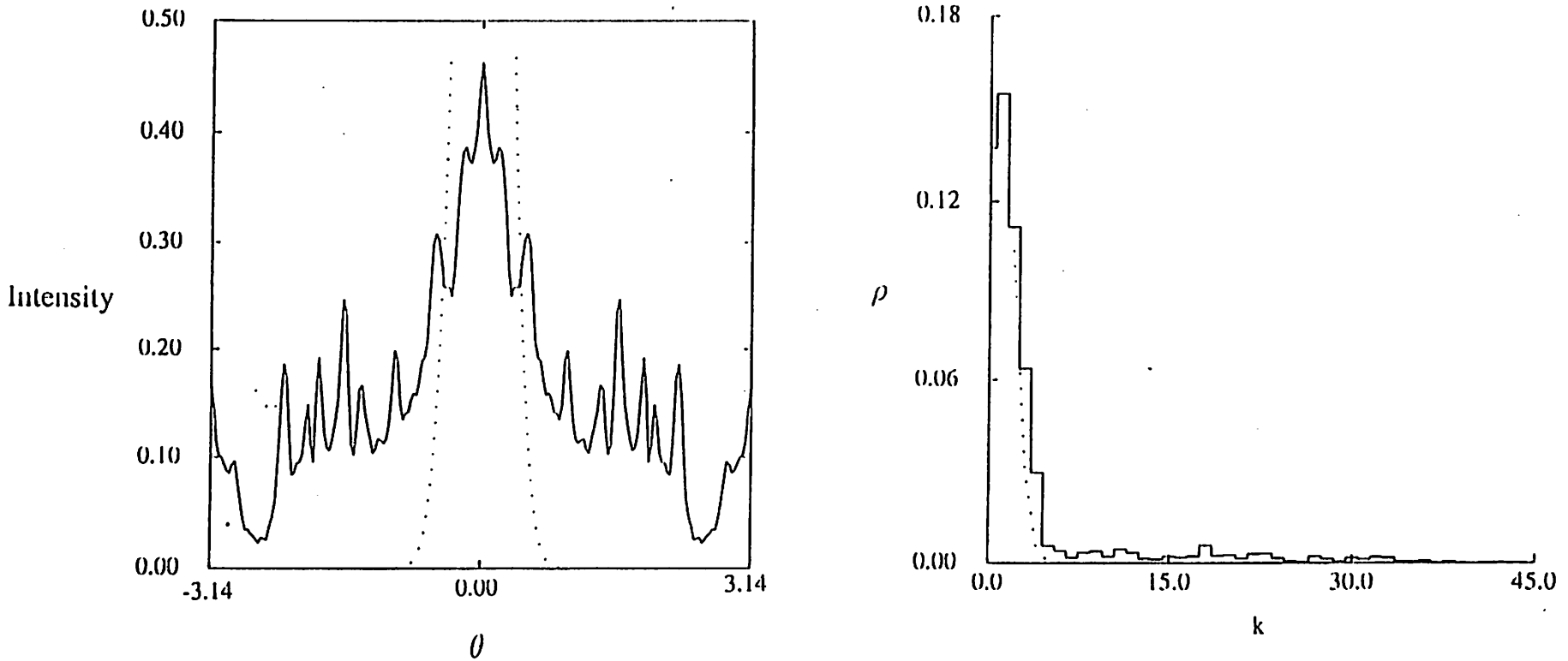
0.50
0.40
0.30
0.20
0.10
0.00
Intensity
-3.14
0.00
3.14
θ
0.18
0.12
0.06
0.00
ρ
0.0
15.0
30.0
45.0
k

(b)

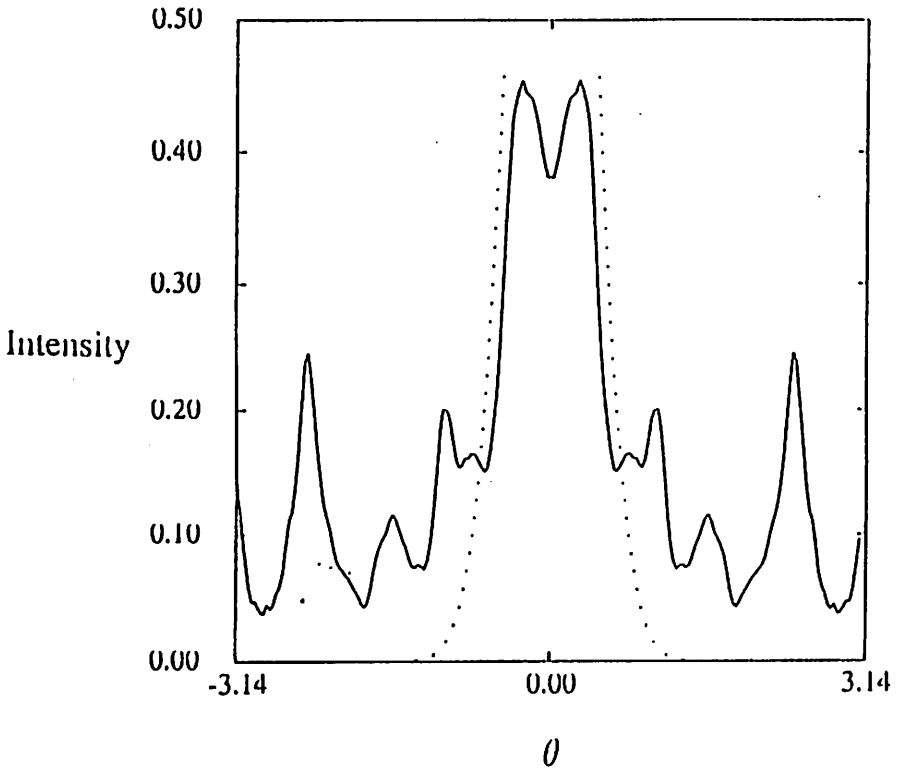
0.50
0.40
0.30
0.20
0.10
0.00
Intensity
-3.14
0.00
3.14
θ

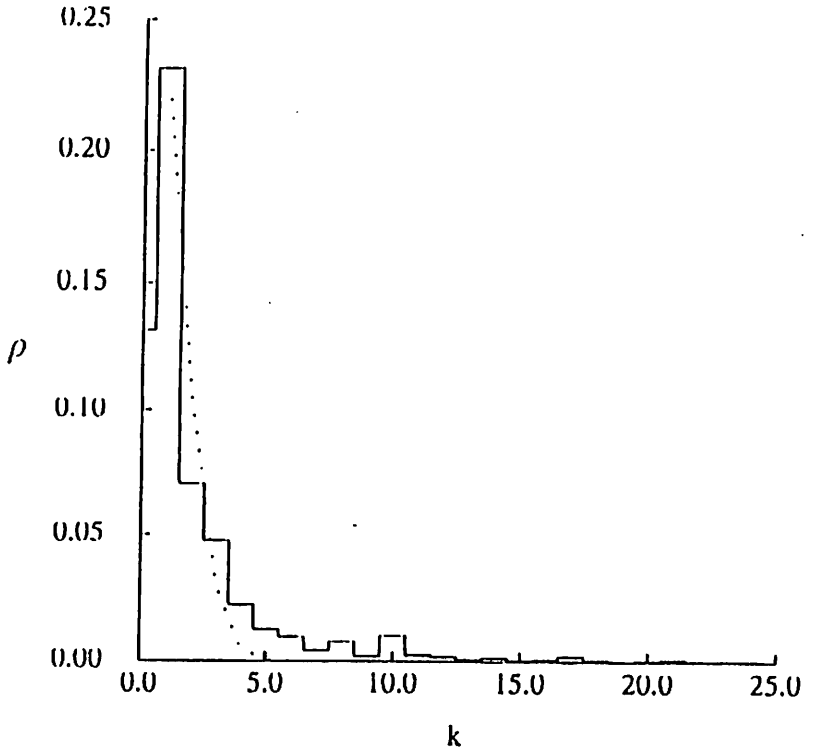
0.25
0.20
0.15
0.10
0.05
0.00
ρ
0.0
5.0
10.0
15.0
20.0
25.0
k

(c)

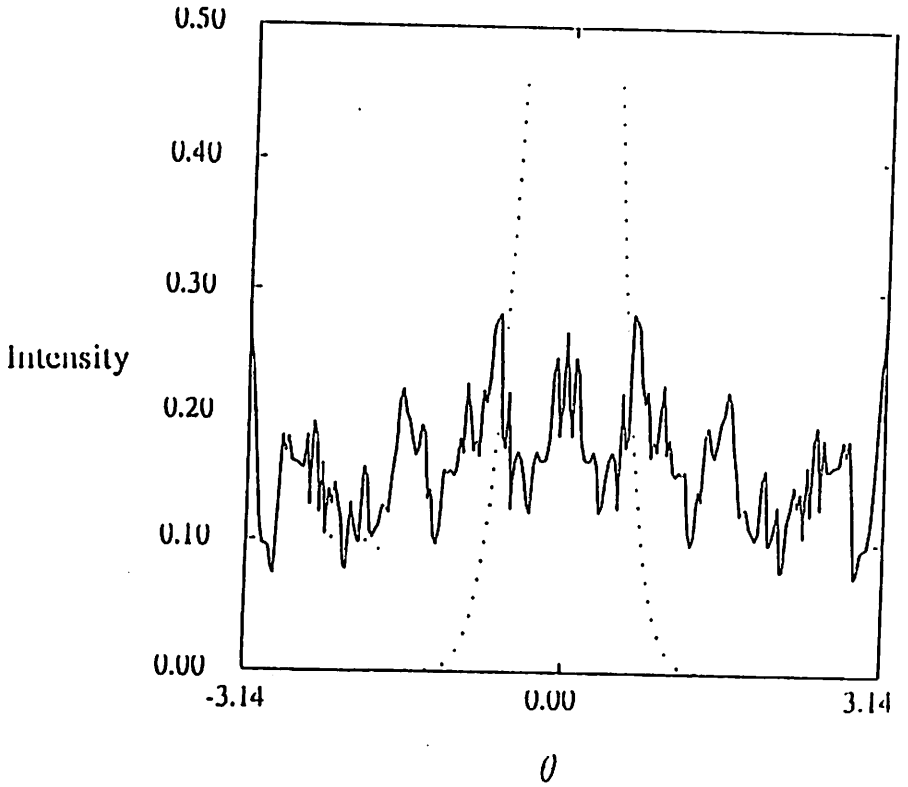
0.50
0.40
0.30
0.20
0.10
0.00
Intensity
-3.14
0.00
3.14
θ

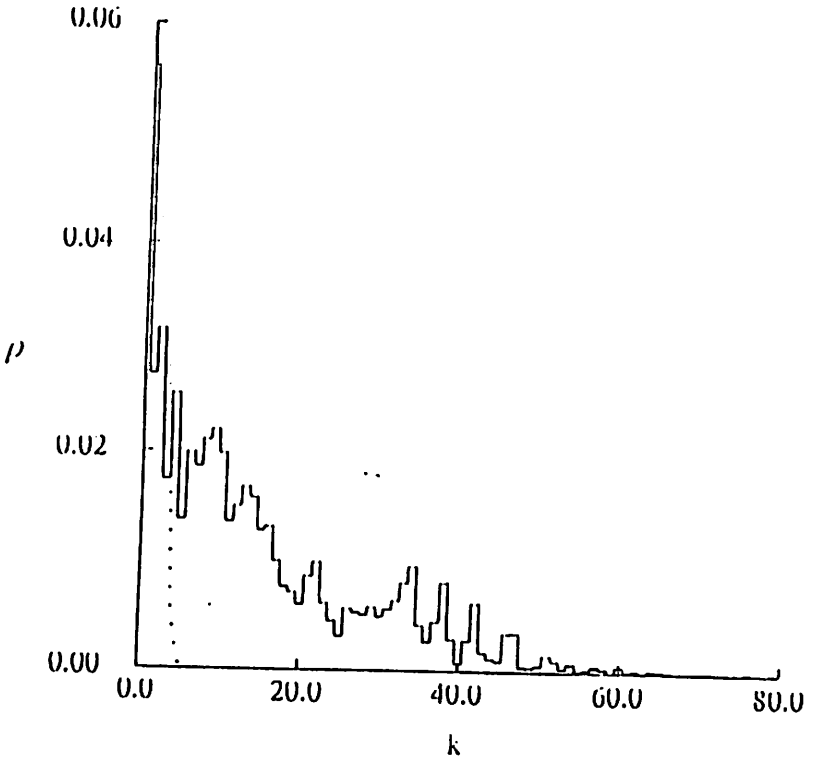
0.06
0.04
0.02
0.00
P
0.0
20.0
40.0
60.0
80.0
k

(a)

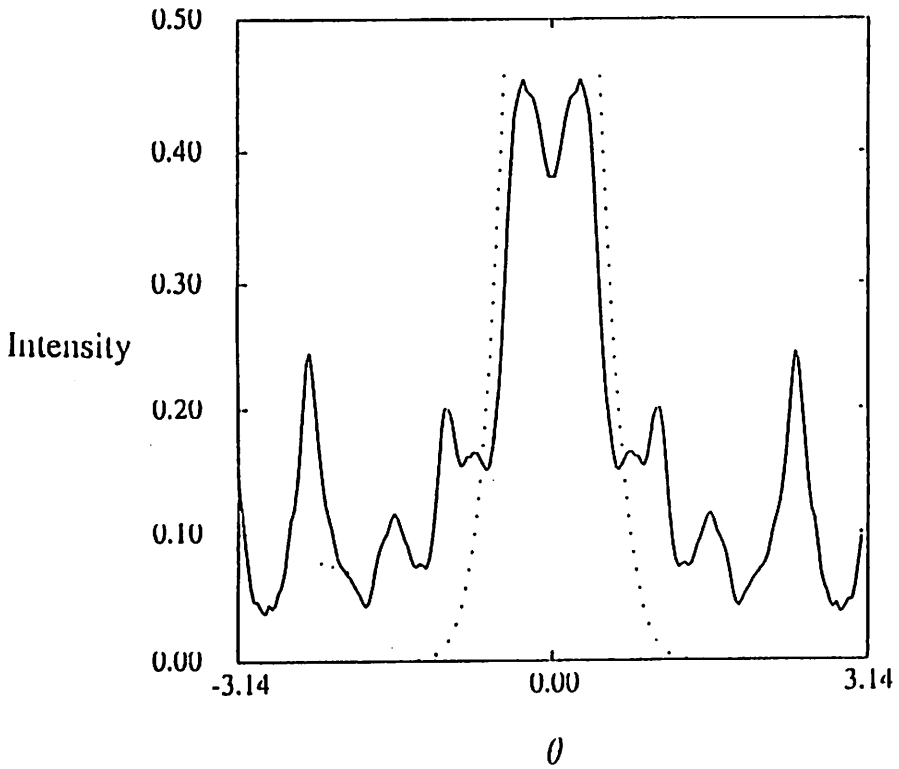
0.50
0.40
0.30
0.20
0.10
0.00
Intensity
-3.14
0.00
3.14
θ

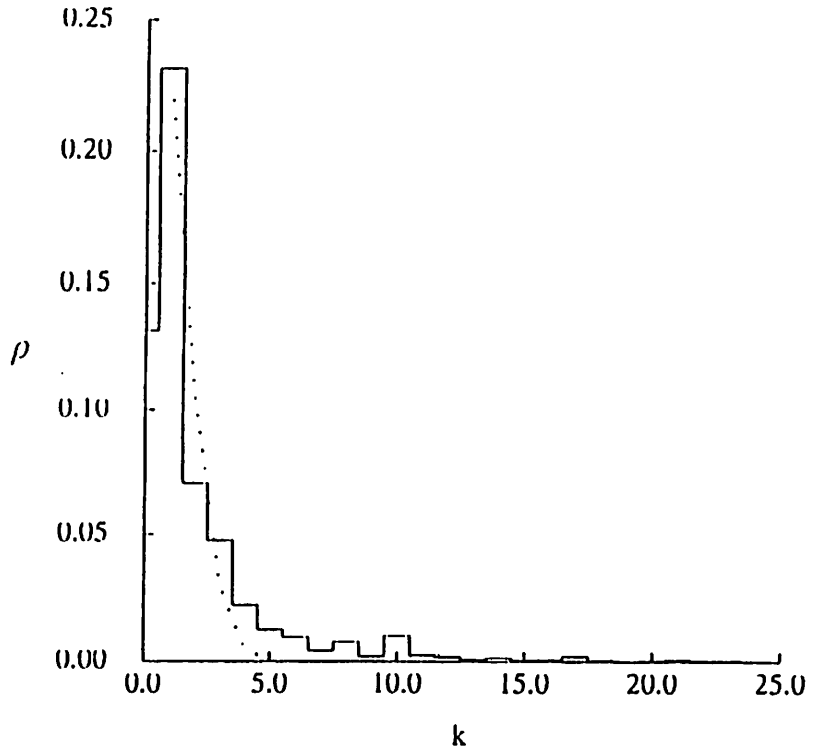
0.25
0.20
0.15
0.10
0.05
0.00
ρ
0.0
5.0
10.0
15.0
20.0
25.0
k

(b)

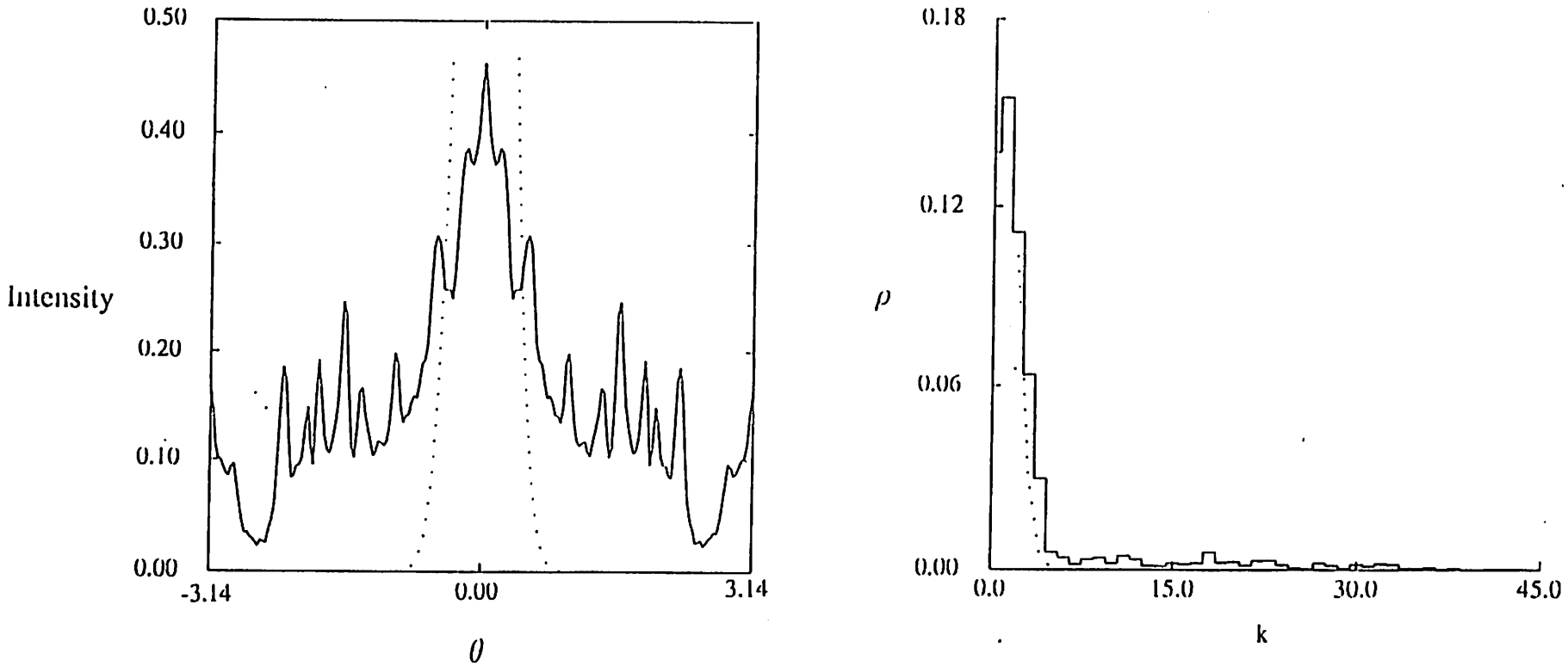
0.50
0.40
0.30
0.20
0.10
0.00
Intensity
-3.14
0.00
3.14
θ
0.18
0.12
0.06
0.00
ρ
0.0
15.0
30.0
45.0
k

(d)

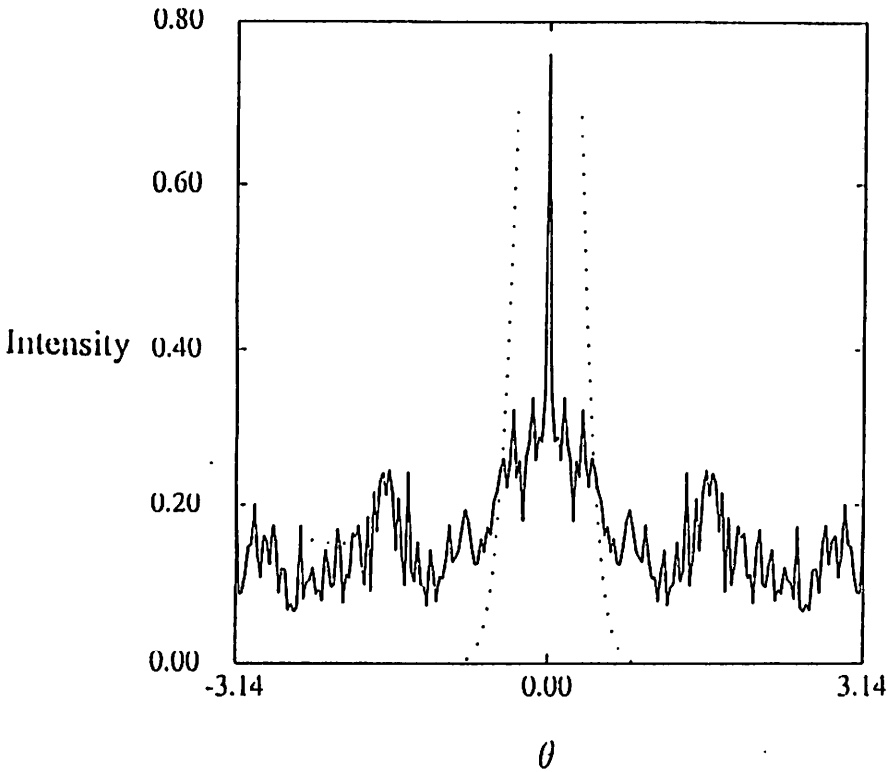
0.80
0.60
0.40
0.20
0.00
Intensity
-3.14
0.00
3.14
θ

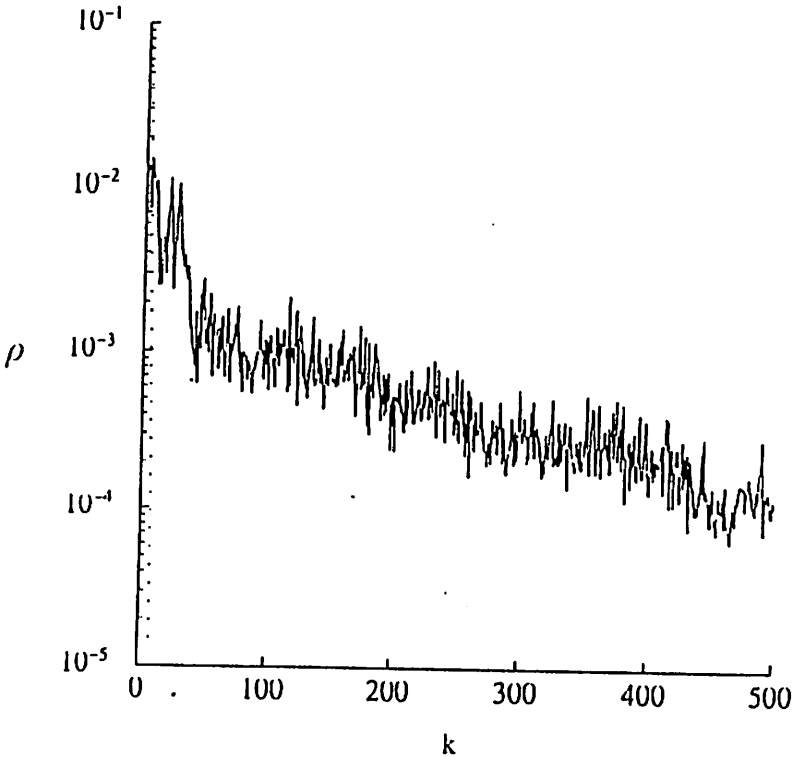
10⁻¹
10⁻²
10⁻³
10⁻⁴
10⁻⁵
ρ
0
100
200
300
400
500
k

(a)

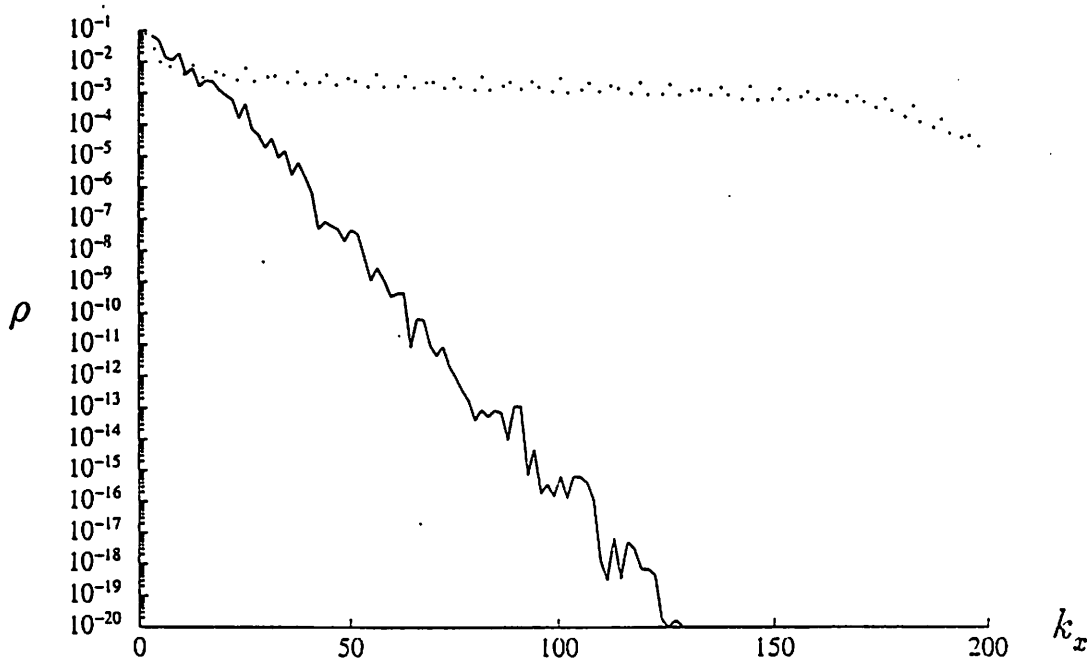
ρ
10^{-1}
10^{-2}
10^{-3}
10^{-4}
10^{-5}
10^{-6}
10^{-7}
10^{-8}
10^{-9}
10^{-10}
10^{-11}
10^{-12}
10^{-13}
10^{-14}
10^{-15}
10^{-16}
10^{-17}
10^{-18}
10^{-19}
10^{-20}
0
50
100
150
200
k_x

(b)

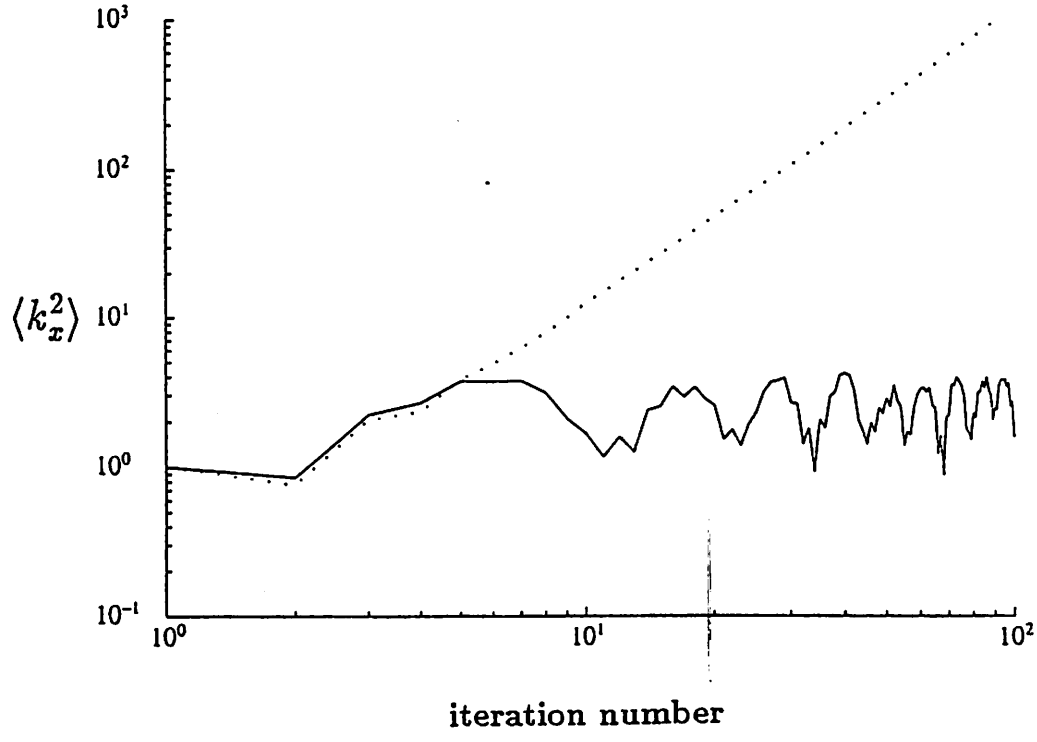
$\langle k_x^2 \rangle$
10^3
10^2
10^1
10^0
10^{-1}
10^0
10^1
10^2
iteration number